IEEE Access
Multidisciplinary ⋮ Rapid Review ⋮ Open Access Journal

Received 14 February 2024, accepted 26 February 2024, date of publication 5 March 2024, date of current version 14 March 2024.

Digital Object Identifier 10.1109/ACCESS.2024.3373784

RESEARCH ARTICLE

Investigation of Dual Coil Induction Heating for Enhanced Temperature Distribution Optimization

DAE YONG UM[1], (Member, IEEE), MIN JAE KIM[2], SEUNG AHN CHAE[3], AND GWAN SOO PARK[3], (Senior Member, IEEE)

[1]School of Engineering, Newcastle University, NE1 7RU Newcastle Upon Tyne, U.K.
[2]Kitchen Appliance Lab, LG Electronics, Changwon-si 51533, South Korea
[3]Department of Electrical and Computer Engineering, Pusan National University, Busan 46241, South Korea

Corresponding author: Gwan Soo Park (gspark@pusan.ac.kr)

This work was supported by the Technology Innovation Program (Development of real-time monitoring sensor for gas pipe) funded by the Ministry of Trade, Industry and Energy (MOTIE, South Korea) under Grant RS-2022-00154902.

ABSTRACT Optimizing temperature distribution is one of the crucial tasks in induction heating technology, especially, for small devices with constraints on compactness, efficiency, and cost. The optimization solely using coil shape parameters, referred to as 'traditional coil design', cannot provide a satisfactory solution with highly limited structural constraints of lateral or vertical size. A multi-coil system where each set of coils is fed by multiple inverters enables control of the magnitude and phase of exciting currents, providing an alternative approach to enhance the design flexibility. However, additional inverters increase both the volume of a driving circuit and the cost of products, so this approach has a risk of reducing applicability to personal electronics. This article proposes a dual coil system, consisting of primary and secondary coils, to enhance the flexibility for temperature distribution optimization. The impact of primary and secondary coil currents on heat source distribution and efficiency are analyzed, and an equivalent circuit model representing both coils and a workpiece is introduced to provide the main concept of the proposed dual coil system. The effect of circuit parameters on resonance characteristics of the dual coil system are studied for a sensitivity analysis of design parameters. Finally, the optimization flow is proposed and applied to a case study model to demonstrate its superiority compared to the traditional coil design. Potential challenges are discussed to provide insights for further model development.

INDEX TERMS Induction heating, optimization, resonant characteristics, solenoidal coil, temperature distribution, wireless power transfer.

I. INTRODUCTION

Induction heating (IH) technology is widely adopted in domestic, industrial, and medical applications. Nowadays, it is currently becoming preferred in personal electronics and small devices (e.g., electronic cigarettes and metal casting) for the replacement of a traditional electrical heating method. The increasing utilization of IH technology in these applications necessitates a meticulous design optimization process focused on miniaturization, high efficiency, rapid heating, and cost-effectiveness. Furthermore, the optimization for achieving a desired temperature distribution on the heating surface is a task essential for enhancing the applicability of IH technology.

The temperature distribution optimization can be conducted by two sequent steps of a transient thermal and time-harmonic magnetic finite element analysis (FEA) in Fig. 1 and the optimization process is as follows: First, the workpiece is segmented into sections with a given heat source, and the temperature distribution along the line or surface of the workpiece is calculated at the target time using the transient thermal analysis. This information is then used to evaluate the objective function such as the root mean square error (RMSE), and an optimization algorithm determines the

The associate editor coordinating the review of this manuscript and approving it for publication was Sawyer Duane Campbell.

TABLE 1. Drawbacks of existing IH system design for temperature distribution optimization.

Design approach	Drawbacks
Traditional IH coil design [1] – [6]	· High design constraints · Low power density · Low efficiency · Fixed temperature distribution
Multi-coil IH system [7] – [9]	· Increase cost and the volume of electronic circuit · Increase control complexity

optimal heat source for each section. Based on the obtained heat-source distribution, IH coils can be optimized to find the optimal combinations of coil geometries, amplitude, and phase of currents flowing through each coil.

Over the last decades, many studies have employed a coil-shape design and a multi-coil system for IH optimization. The coil shape design involves changing the structural design variables that can influence the heat-source distribution [1], [2], [3], [4], [5], [6]. Byun et al. proposed an optimal coil design process for a domestic IH cooker, achieving a uniform temperature distribution [1]. The Levenberg-Marquardt method was adopted to find the optimal coil shape with a corrected heat transfer coefficient to increase the fidelity of the model. However, a reduced number of turns resulted in a decreased steady-state temperature on the pan, degrading the efficiency. Boadi et al. suggested optimal coil structures [3], but without structural constraints, the results may not be suitable for small devices designed with high structural constraints of lateral and vertical size. Another approach, a multi-coil system, can be a suitable way for IH optimization with these high structural constraints. This method consists of multiple coils fed by each inverter [7], [8], [9]. This method allows individual control of currents supplied to coil sets, offering a flexible optimization of the heat-source distribution. Ngoc et al. proposed a phase control method of multiple inverter systems for a zone-control IH system [7]. The transfer function of the current phase angle was theoretically derived to achieve the uniform temperature distribution on a workpiece. However, the use of additional inverters poses challenges for small device applications due to increased costs and limited circuit board space. Therefore, these aspects are a bottleneck for enhancing the availability of IH technology. The briefly described drawbacks of existing approaches are summarized in Table 1.

This article investigates a method for realizing a multi-coil system without extra inverters, based on the theory of wireless power transfer (WPT). In this approach, the secondary coil is energized by the primary coil, enabling diverse heat source distributions through different combinations of primary and secondary coil currents. The concept of this method has been discussed in some literatures [10], [11], and [12]. In [10], the secondary coil above the primary planar coil, connected to the capacitor in series, was employed to make the uniform temperature distribution using a single inverter. The same configuration was adopted to realize a robust IH for enhancing the adaptation to variable-sized loads and horizontal/vertical displacements [11]. The authors have mainly focused on the feasibility of a dual-coil IH system, not from the optimization point of view. To extend this method for a variety of targets and scenarios, more generalized-optimal design procedures should be investigated, and this article extends the discussion beyond the feasibility to address the optimization aspect.

This article is organized as follows. Section II illustrates the concept of the dual-coil IH system for heat-source control and evaluates the impact of primary and secondary coil currents on the heat-source distribution. The magnitude of the ratio of the secondary coil to the primary coil is referred to as the 'current ratio', and its phase is referred to as the 'phase difference'. An objective function is then defined and calculated in Section II to quantitatively analyze the effects of the current ratio and phase difference on objective function values. Section III presents a dual coil system illustrated by using a simplified equivalent circuit representing both coils and the workpiece. Resonance characteristics of the dual-coil system are studied with design parameters' sensitivity to guide the selection of design variables in the optimization procedure. Section IV proposes an optimization procedure for the temperature distribution, considering efficiency. The proposed algorithm is applied to a case study model, and the results are compared with those obtained through optimization only relying on the coil geometry. Finally, potential challenges arising from temperature-dependent resistivity and magnetic non-linearity are discussed in Section V, providing comprehensive insights for future research to enhance stability and reproducibility.

II. DUAL-COIL IH SYSTEM

The dual-coil IH system in this study is comprised of two sets of solenoidal coils, where N_1 and N_2 denote the number of turns of the primary and secondary coil sets, respectively, as illustrated in Fig. 2(a). The workpiece, with a diameter of 10 mm, a height of 30 mm, and a thickness of 0.5 mm, is positioned within coils. Due to structural constraints, only a single-layer coil is permitted, and the allowable number of turns (N_t) is restricted by vertical structural consideration (h_{lim}). As a case study example for achieving the uniform temperature of 150°C along the workpiece after a 10-second heating duration, the required heat source for each section can be determined using optimization methods in transient thermal analysis, expressed as:

$$\rho C_p \frac{\partial T}{\partial t} - \nabla \cdot (k \nabla T) = q \tag{1}$$

where ρ, C_ρ, T, k, and q represent the density, specific heat, temperature, heat conductivity, and heat-source density of each material, respectively [13].

For this study, the workpiece was axially divided into 16 sections (8 × 2 symmetry), as shown in Fig. 2(b). The optimal heat source for each section, ensuring a uniform

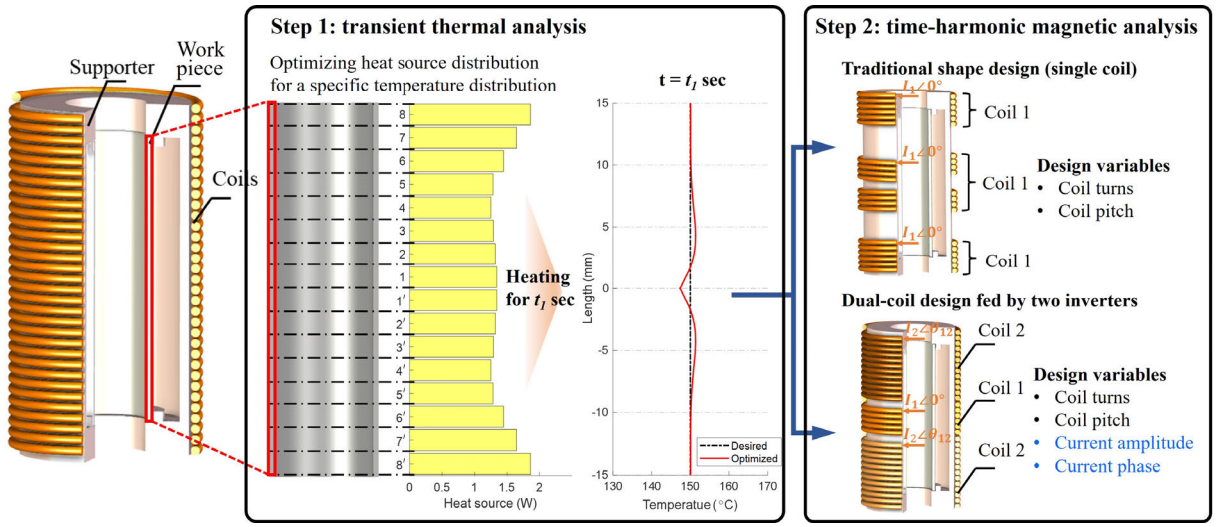

FIGURE 1. The overview of temperature distribution optimization.

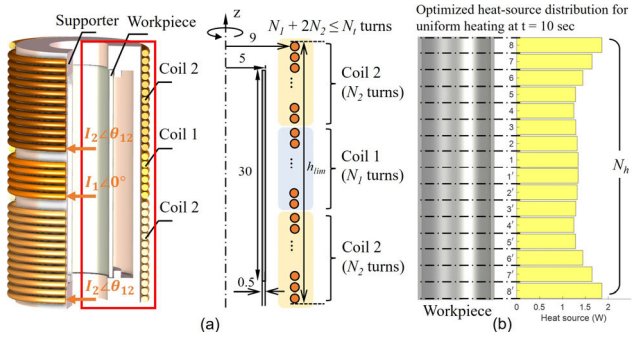

FIGURE 2. (a) Structure of the dual-coil IH system and (b) the required heat-source distribution for uniformly heating of the workpiece at 10 seconds.

TABLE 2. Thermal properties used in thermal simulations.

Material	Specific heat	Thermal conductivity	Density
SPCC (workpiece)	480 J/(kg·K)	56 W/(m·K)	7850 kg/m^3
Copper (Coil)	385 J/(kg·K)	400 W/(m·K)	8960 kg/m^3
PEEK (Supporter)	1390 J/(kg·K)	0.25 W/(m·K)	1300 kg/m^3

temperature distribution at 10 seconds, is determined using the Method of Moving Asymptotes (MMA) implemented in COMSOL Multiphysics [14]. The thermal properties used in thermal simulations are summarized in Table 2. The calculated heat source distribution can be theoretically predictable, with the edge of the workpiece requiring a higher heat source due to increased heat loss toward the nearby support structure.

In the depicted study model (Fig. 2(a)), the current ratio, $|I_2/I_1|$ and phase difference, θ_{12} are defined as the magnitude and phase components of the ratio of the secondary current I_2 to the primary current I_1, respectively. Fig. 3 shows the heat-source distribution according to $|I_2/I_1|$ and θ_{12} with N_1 and N_2 set to 16 and 8, respectively.

In Fig. 3(a), each coil set can influence the location of the heat source towards the center or edge when the currents flow in phase and their ratio varies from $|I_2/I_1| = 0$ to $|I_2/I_1| = 10$. Consequently, the combination of current magnitudes can determine various heat source distributions. However, isolating heat-source within a target area shows a challenge when relying on current magnitudes.

Fig. 3(b) depicts the effect of the phase difference θ_{12} on the heat source distribution when $|I_2/I_1|$ is fixed to 2. When currents of each set flow in opposite directions ($\theta_{12} = 180°$), it localizes the heat source toward the edge of the workpiece due to the magnetic field generated by each coil shielding each other. While the phase difference provides flexibility in achieving various heat source distributions, as shown in Fig. 3(b), it requires careful consideration due to the potential risk of efficiency degradation due to reduced heat-source.

To quantitatively investigate the influence of $|I_2/I_1|$ and θ_{12} on the heat source distribution, an objective function $f(\boldsymbol{x})$ and efficiency η are defined as follows:

$$f(\boldsymbol{x}) = \sqrt{\frac{1}{N_h}\sum_{i=1}^{N_h}\left(\frac{Q_i}{Q_{req,i}} - 1\right)^2} \tag{2}$$

$$\eta = \frac{\sum_{i=1}^{N_h} Q_i}{\sum_{i=1}^{N_h} Q_i + \left|\bar{I}_1\right|^2 R_1 + \left|\bar{I}_2\right|^2 R_2}. \tag{3}$$

Here, ideal combinations of the heat source can minimize the objective function $f(\boldsymbol{x})$ to be 0. The variable $\boldsymbol{x}$ represents a set of design variables, N_h is the number of sections of the workpiece, Q_i and $Q_{req,i}$ are the calculated heat source and the required heat source at the i-th section of the workpiece, respectively. R_1 and R_2 are the resistance of the primary and

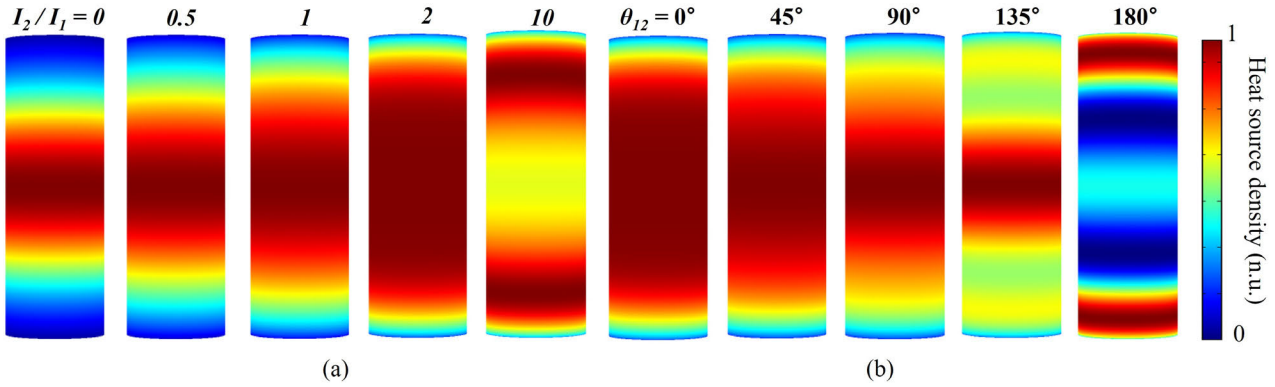

FIGURE 3. The effect of (a) current ratio (I_2/I_1) when $\theta_{12} = 0°$ and phase difference (θ_{12}) when $I_2/I_1 = 2$ on the heat-source distribution of the workpiece. Each result is normalized to its maximum value.

secondary coils, including AC losses of Litz-wire due to both skin effect and proximity effect [15].

Fig. 4 presents objective function values and the efficiency for two different coil arrangements in a $|I_2/I_1| - \theta_{12}$ plane. The objective function can be calculated by using the heat-source profile as shown in Fig. 2(b) as $Q_{req,i}$ in equation (2). The objective function values exhibit more than one minimum point (two local minima in Fig. 4). The minimum points and values of the objective function vary according to the coil arrangement, as depicted in Fig. 4(a) and (b). Each minimum point is positioned in the region of phase differences both lower and higher than 180°, exhibiting different values. This result shows combinations of $|_2/I_1| - \theta_{12}$ can make local optima. Consequently, the identification of a global optimum or defining proper constraints is imperative to select the most effective heat-distribution. Additionally, the efficiency must be carefully considered during optimal point selection, as the efficiency at the optimal point is below 80%, which indicates that exclusive pursuit of the optimal temperature distribution can sacrifice efficiency. Therefore, establishing constraints to guarantee an acceptable efficiency is indispensable in this optimization process. The efficiency as shown in Fig. 4 tends to decrease when θ_{12} is close to 180° due to a reduced heat-source (the null area as depicted as Fig. 3(b)). Thus, higher efficiency can be enhanced by deviating the feasible θ_{12} from 180° and iteratively seeking the optimal solution until the lower limit of the efficiency is satisfied.

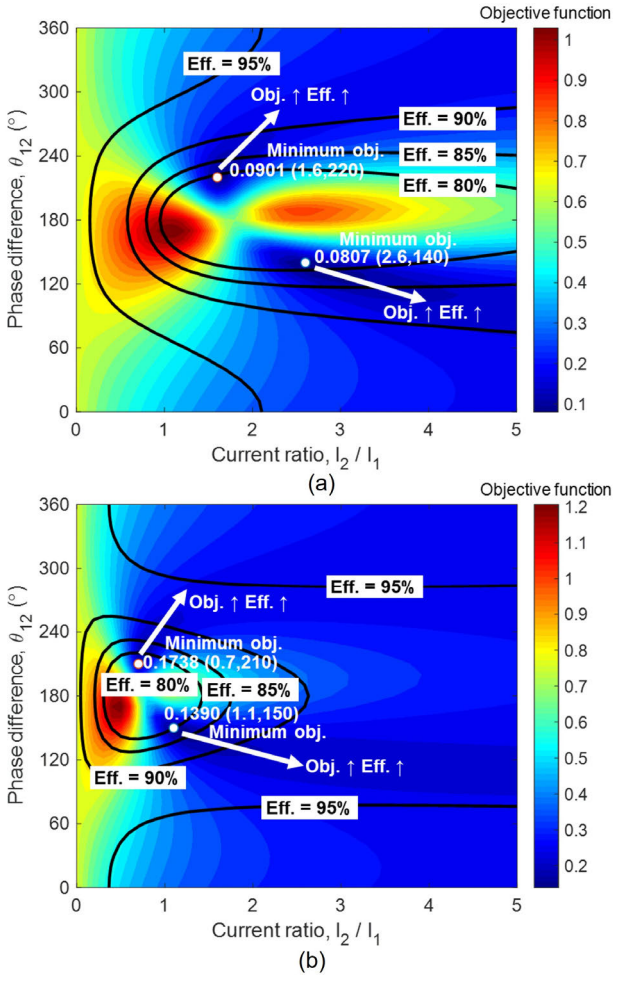

FIGURE 4. The objective function values and efficiency according to $|I_2/I_1|$ and θ_{12} with two coil arrangements: (a) $N_1 = 16$, $N_2 = 8$, (b) $N_1 = 10$, $N_2 = 11$.

III. RESONANCE CHARACTERISTICS

In this article, an efficient alternative approach that can eliminate the need for additional inverters is proposed by finely tuning resonance characteristics of both the primary and secondary systems. As depicted in Fig. 5, a voltage-driven source is connected in series with a compensation capacitor to the primary coil, while the secondary coil is similarly linked to a distinct compensation capacitor in series. This configuration mirrors a series-series topology used in inductive power transfer, except for accounting for the eddy current behavior within the workpiece. The circuit elements include the resistance (R_1, R_2, R_e), compensation capacitor (C_1, C_2), self-inductance (L_1, L_2, L_e), and mutual inductance (M_{1e}, M_{12}, M_{2e}). From the circuit of Fig. 5, voltage equations

with respect to each loop can be expressed as:

$$\bar{V}_i = \left(\bar{Z}_{11} + \frac{1}{j\omega C_1}\right)\bar{I}_1 + j\omega M_{12}\bar{I}_2 + j\omega M_{1e}\bar{I}_e \quad (4)$$

$$0 = \left(\bar{Z}_{22} + \frac{1}{j\omega C_2}\right)\bar{I}_2 + j\omega M_{12}\bar{I}_1 + j\omega M_{2e}\bar{I}_e \quad (5)$$

$$0 = (R_e + j\omega L_e)\,\bar{I}_e + j\omega M_{1e}\bar{I}_1 + j\omega M_{2e}\bar{I}_2. \quad (6)$$

where $\bar{Z}_{11} = R_1 + j\omega L_1$ and $\bar{Z}_{22} = R_2 + j\omega L_2$ are the self-impedance of the primary and secondary coils, respectively. Combing (6) into (4) and (5), the voltage equations of the primary and secondary coils can be written as follows:

$$\bar{V}_i = \left(\bar{Z}_{11} + \frac{1}{j\omega C_1} + \frac{\omega^2 M_{1e}^2}{R_e + j\omega L_e}\right)\bar{I}_1 + \left(j\omega M_{12} + \frac{\omega^2 M_{1e}M_{2e}}{R_e + j\omega L_e}\right)\bar{I}_2 \quad (7)$$

$$0 = \left(\bar{Z}_{22} + \frac{1}{j\omega C_2} + \frac{\omega^2 M_{2e}^2}{R_e + j\omega L_e}\right)\bar{I}_2 + \left(j\omega M_{12} + \frac{\omega^2 M_{1e}M_{2e}}{R_e + j\omega L_e}\right)\bar{I}_1 \quad (8)$$

The first term and the second term of right side in (7) and (8) presents that the self-impedance and mutual inductance of each coil can be replaced by an equivalent resistance ($R_{eq,1}$, $R_{eq,2}$), self-inductance ($L_{eq,1}$, $L_{eq,2}$), and complex mutual inductance $\bar{M}_{12}$ including the workpiece, written as:

$$R_{eq,i} = R_i + \frac{\omega^2 M_{ie}^2}{R_e^2 + (\omega L_e)^2}R_e \quad \forall i = 1, 2 \quad (9)$$

$$L_{eq,i} = L_i - \frac{\omega^2 M_{ie}^2}{R_e^2 + (\omega L_e)^2}L_e \quad \forall i = 1, 2 \quad (10)$$

$$\bar{M}_{12} = M_{12} + \frac{\omega^2 M_{1e}M_{2e}}{R_e^2 + (\omega L_e)^2}\left(-j\frac{R_e}{\omega} - L_e\right) \quad (11)$$

where the workpiece increases the resistance but decreases the inductance. Moreover, the mutual coupling between coils includes both resistive and inductive components. As a result, the original circuit on the left side of Fig. 5 can be more simplified to that on the right side.

From the simplified circuits, the current ratio of the secondary current to the primary current can be obtained by rearranging (8) and expressed as:

$$\frac{\bar{I}_2}{\bar{I}_1} = \frac{-j\omega\bar{M}_{12}}{R_{eq,2} + j\omega L_{eq,2}\left\{1 - (\omega_{r2}/\omega)^2\right\}} \quad (12)$$

$$\omega_{r,i} = 1\Big/\left(L_{eq,i}C_i\right)^{1/2} \quad \forall i = 1, 2. \quad (13)$$

The equation (12) includes mutual inductance $\bar{M}_{12}$ in the numerator, the secondary circuit elements ($R_{eq,2}$, $L_{eq,2}$), and a ratio of the driving frequency to the secondary resonant frequency of (13), which is a function of the inverse of ω/ω_{r2} in its denominator of (12). That is, three characteristics of frequency dependent current ratio I_2/I_1 can be predictable. First, the coil arrangement of the primary and secondary coils such as number of turns and its position can determine the current ratio as these variables vary the mutual coupling and the secondary circuit elements. Secondly, the current ratio is independent of a resonant frequency of the primary side circuit, which can be neglected during the process of heat-source distribution optimization. Consequently, the resonant frequency of the primary circuit ω_{r1} and the corresponding compensation capacitor can be used to control the input power without compromising the pre-optimized heat-source distribution.

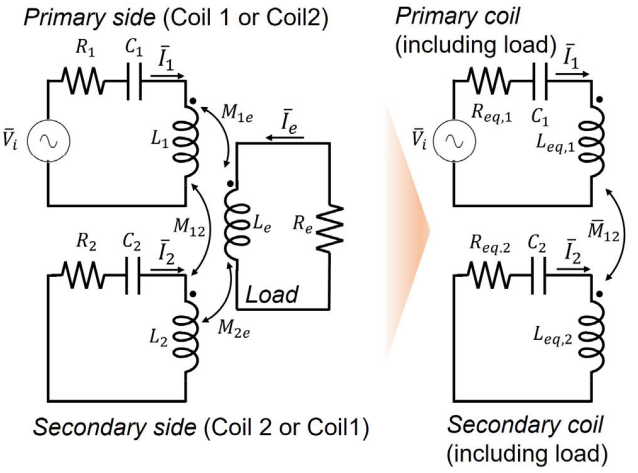

FIGURE 5. The simplified equivalent circuit of dual-coil IH system.

To discuss the characteristic of I_2/I_1 quantitatively, the time-harmonic magnetic FEA was used to for simulation studies. The structure of the model is presented in Fig. 2(a), and the material properties of the workpiece are given by an electrical conductivity of 8 MS/m and a relative permeability of 100. The number of turns in the coil 1 and coil 2 are 16 and 8, respectively. Then, the compensation capacitors (C_1, C_2) are tuned according to resonant frequencies (ω_{r1}, ω_{r2}).

Fig. 6 presents the resonant characteristics of $|I_2/I_1|$ with the different resonant frequency of the secondary circuit, ranging from 40 kHz to 100 kHz, while the resonant frequency of the primary circuit is fixed to 80 kHz. In Fig. 6(a) and (b), coil 1 is connected to the primary and secondary circuits, respectively. The current ratio $|I_2/I_1|$ at the resonant frequency ω_{r2} is rarely sensitive to the driving frequency, ranging from 40 kHz to 200 kHz, which is over the bandwidth of the circuit. Its amplitude can be predicted by assuming equations (9) and (11), neglecting coil resistance (R_1, R_2), and considering equal magnitudes of resistive and inductive components in the workpiece ($R_e = \omega L_e$) in high frequencies [16]. Then, the current ratio $|I_2/I_1|$ at ω=ω_{r2} can be approximated by

$$\frac{\bar{I}_2}{\bar{I}_1} = -j\frac{M_{12}L_e}{M_{2e}^2} - \frac{M_{1e}}{M_{2e}}(1 - j) \quad (14)$$

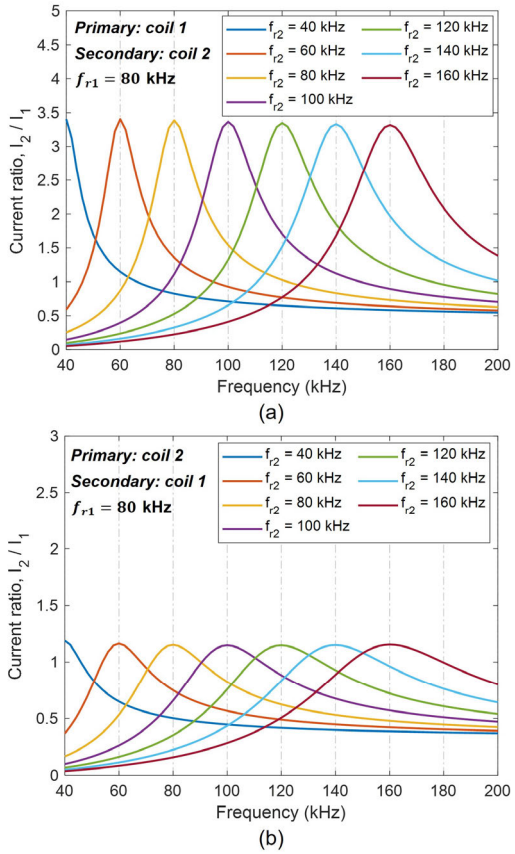

FIGURE 6. The resonance characteristic of $|I_2/I_1|$ with the different secondary resonant frequency: (a) coil 1 (primary) and coil 2 (secondary), (b) coil 2 (primary) and coil 1 (secondary).

where the magnitude and phase in (14) are independent of the frequency. Additionally, $|I_2/I_1|$ converges to a certain value, determined solely by the coil geometry, given as

$$\frac{\bar{I}_2}{\bar{I}_1} \cong 0 \,(\omega \ll \omega_{r2}) \tag{15}$$

$$\frac{\bar{I}_2}{\bar{I}_1} \cong \frac{-M_{12}L_e + M_{1e}M_{2e}(1+j)}{L_2L_e - M_{2e}^2(1+j)} \,(\omega \gg \omega_{r2}) \tag{16}$$

Here, current ratio at specific condition of (14), (15) and (16) is determined by mutual inductances between primary and secondary circuits, so it explains that the frequency response of the current ratio varies qualitatively as the primary circuit is shifted from coil 1 to coil 2, as shown in Fig. 6(a) and (b).

Fig. 7 shows the resonant characteristic of $|I_2/I_1|$, θ_{12}, output power, and efficiency with the same condition of Fig. 6(a). The x-axis is the ratio of the driving frequency to the secondary resonant angular frequency ω/ω_{r2}. Both $|I_2/I_1|$ and θ_{12} are clearly overlapped if ω/ω_{r2} is the same regardless of the secondary resonant angular frequency ω_{r2}, as shown in Fig. 7(a) and (b). Thus, the secondary capacitor C_2 can be selected as a variable to determine both $|I_2/I_1|$ and θ_{12} when the driving frequency is given as a fixed parameter. Fig. 7(c) shows the frequency-dependence of the output power, exhibiting a large difference between two peak values. This difference arises because the phase difference θ_{12} in Fig. 7(c) approaches to 180°, where opposite currents in each coil can shield their magnetic fields, resulting in decreasing the heat-source and an equivalent output resistance. Moreover, the decrease of equivalent resistance represents a dominance of coil losses and a degradation of the efficiency, as presented in Fig. 7(d). In conclusion, drive frequencies $\omega > \omega_{r2}$ should not be considered from the efficiency perspective.

As observed in Fig. 8(a) and (b), both $|I_2/I_1|$ and θ_{12} versus the drive frequency are independent of the primary resonant frequency, as expected in equation (3). In contrast, the primary resonant frequency only affects the output power while sustaining the efficiency, as shown in Fig.8(c) and (d). Thus, the primary capacitor C_1 is selected as a control variable, which enables to achieve the required output power without compromising the heat-source distribution.

The findings in Section III are summarized as follows:

- The secondary capacitor C_2 can be selected as a variable to control the current ratio $|I_2/I_1|$ and phase difference θ_{12} regardless of the drive frequency.
- The drive frequency should be lower than the resonant frequency of the secondary circuit to prevent a dramatic decrease in the efficiency.
- The primary capacitor C_1 is used to determine the output power at the given driving frequency after completing heat-source distribution optimization as both current ratio and phase difference are independent on ω_{r1}.

IV. OPTIMIZATION

This section describes an optimal design procedure and its application to a design example, followed by a comparative analysis of the proposed design against a solitary coil shape design in terms of efficiency as well as achievable objective function values for the required heat-source distribution.

A. OPTIMIZATION PROCEDURE

The optimization flow of the dual-coil IH system is illustrated in Fig. 9. The design flow is categorized in two steps to attain the desired heat-source distribution and output power, respectively. In the first step, control variables such as the number of turns (N_1, N_2), coil position, and secondary-side capacitor C_2 are chosen for the heat-source distribution optimization. In this step, the primary-side capacitor C_1 is selected as a fixed variable, and the primary circuit is connected to a current source of I_1. Then, the optimization algorithm such as the particle swarm optimization (PSO), genetic algorithm (GA) and evolution strategy (ES) can be used to find global optimal variables which has been successfully applied to optimal IH coil design [4], [5], [17]. In this article, Nelder-Mead simplex algorithm implemented in Comsol Multiphysics is employed with constraints [18]. The objective function value and efficiency are calculated, and the efficiency constraint $g_1(\boldsymbol{x})$,

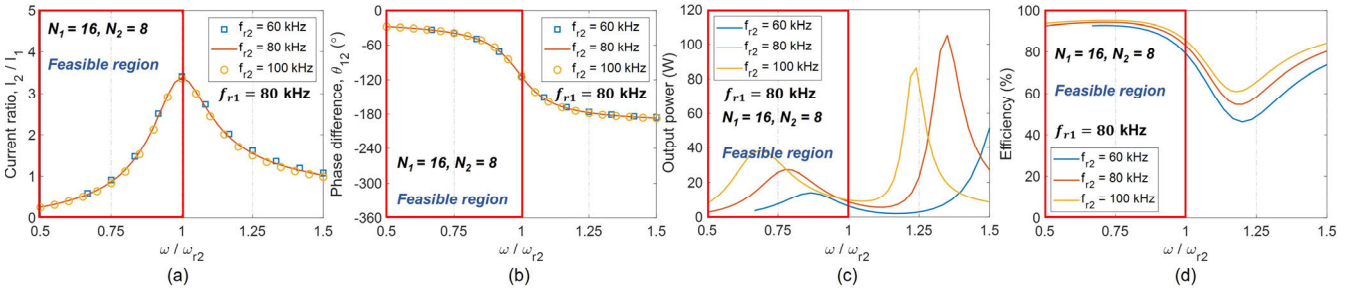

FIGURE 7. The resonance characteristic with different secondary resonant frequencies: (a) $|I_2/I_1|$, (b) θ_{12}, (c) output power, (d) efficiency.

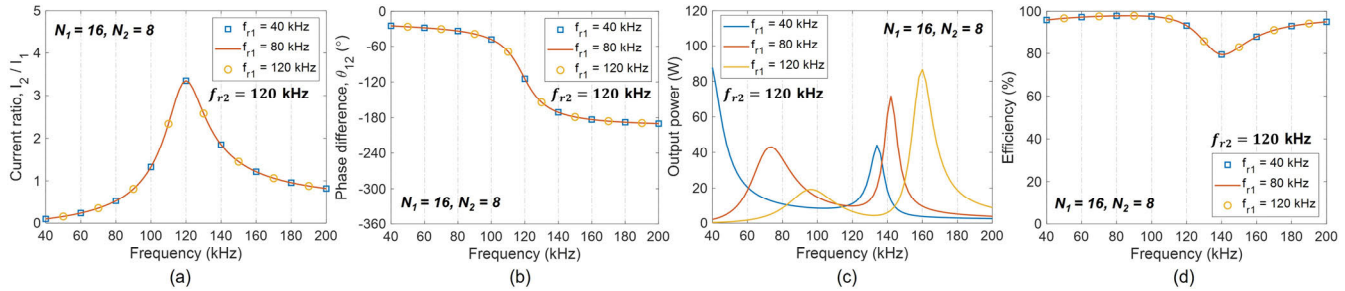

FIGURE 8. The resonance characteristic with different primary resonant frequencies: (a) $|I_2/I_1|$, (b) θ_{12}, (c) output power, (d) efficiency.

imposed to guarantee the efficiency limit η_{lim}, is satisfied as:

$$g_1(\boldsymbol{x}) = \eta_{lim} - \eta_{cal}^{(k)} \leq 0. \tag{17}$$

In a case that the calculated efficiency at the k-th iteration $\eta_{cal}^{(k)}$ does not satisfy the efficiency constraints, a penalty is applied to the objective function by adding $|g_1(\boldsymbol{x})|$ multiplied by α. Once the heat-source is optimized, optimal variables $\boldsymbol{x} = (N_1, N_2, C_2,$ coil position) are set. In the second step, the primary circuit is connected of a voltage source of V_1. The variables used in the first step are set as fixed variables, so the output power can be satisfied by adjusting C_1 and V_1. The input voltage is strongly coupled with an electrical circuit requirement. Thus, the voltage V_1 can be set as a given value or lower and upper boundaries, which can be determined by considering the DC voltage and an allowable duty ratio and the voltage range is set as a lower boundary 5 V_p to an upper boundary of $15V_p$. Finally, the process is terminated within output power $P_{req,o}$.

B. RESULTS

To validate an effectiveness of the proposed design, three optimized models were made based on an example model in Fig. 10(a). The first model (model #1) was optimized only by changing the coil geometry, as shown in Fig. 10(b). The second model (model #2) was made by a proposed design flow of Fig. 9, while the efficiency was not considered in the optimization flow, as illustrated in Fig. 11(a). The third model (model #3) was made by the same design procedure of model #2, but the efficiency was considered in the optimization process, as presented in Fig. 12(b).

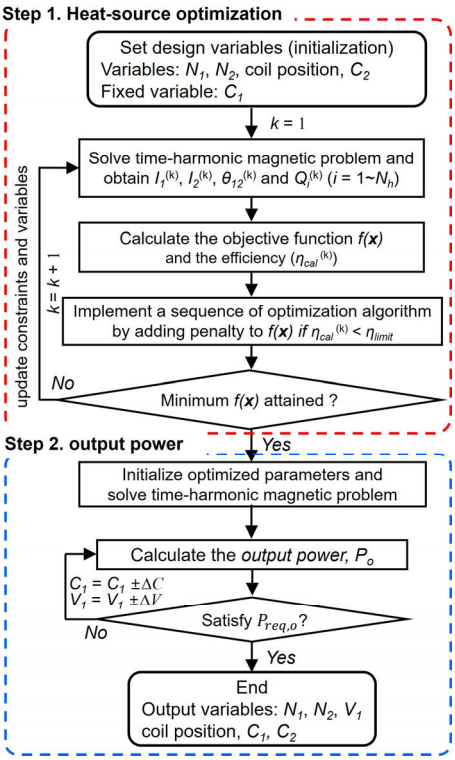

FIGURE 9. Optimization flow for dual coil IH system.

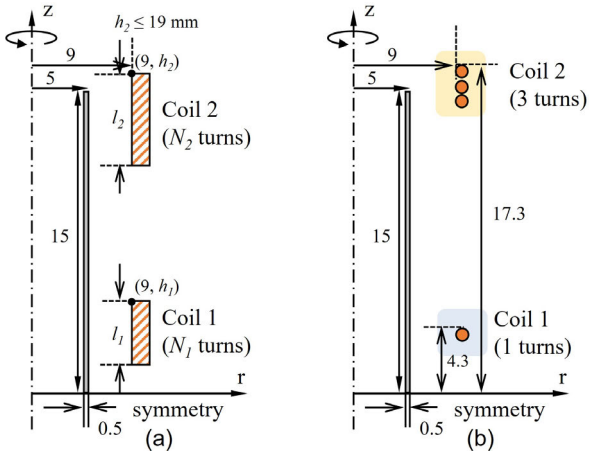

FIGURE 10. The structure of (a) an example model and (b) model #1 (only coil geometry was optimized).

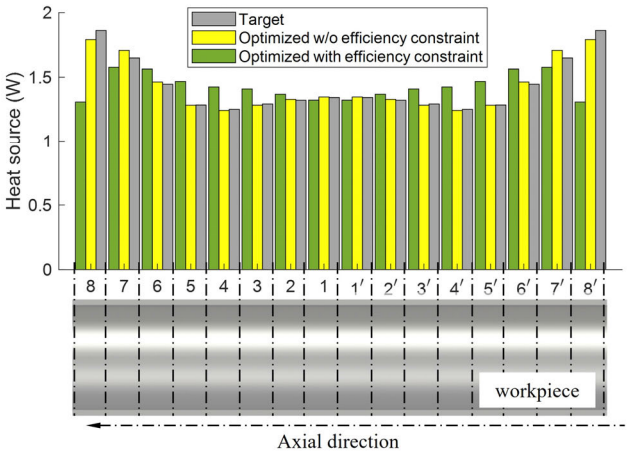

FIGURE 12. Comparison of the heat-source distribution along the workpiece between the model #2 and model #3.

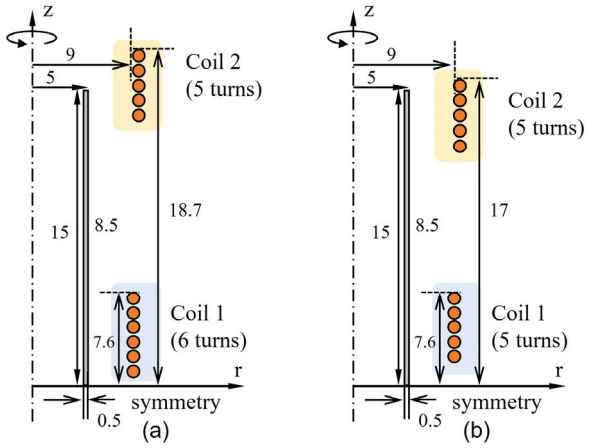

FIGURE 11. The structure of (a) model #2 and (b) model #3, made by a proposed design flow without and with an efficiency constraint, respectively.

In the example model, two set of coils are used, and design variables are the number of coils turns (N_1, N_2) and coil position (h_1, h_2). The upper limit of h_2 is 19 mm, and each coil position constraints are set to prevent coils from being overlapped. In step 1 of a design flow, parameters were given by a current source of 6 A_p, the drive frequency of 100 kHz which is extendable within the frequencies of hundreds kHz where small IH devices adopt, and the lower limit of the efficiency of 88%. The range of variables is N_1 (1∼10) N_2(1∼10), and C_2(100 nF∼4000 nF). In step 2, the target output power was set as 22 W, and the range of variables is C_1(100 nF∼3000 nF) and V_1 (1 V_p ∼15 V_p). Litz wires with one hundred strands of 0.08 mm were used as IH coils and its temperature was set at 50°C. The material properties of the workpiece are given by an electrical conductivity of 4.65 MS/m at 150°C and a relative permeability is set as 100. The design objective is to find circuit and coil shape parameters for the uniform temperature distribution along the workpiece, divided axially into 16 segments ($N_h = 16$) in Fig. 2(b).

Optimized coil arrays in Fig. 10(b) are distributed much more sparsely, compared with the optimized coil arrays in Fig. 11(a). Fig. 11(b) shows that the optimized dual-coil array can be changed when the efficiency is considered in the design flow. The number of turns decreases, but the coil 2 is moved toward inside edge of the workpiece. More detailed results can be seen in Table 3. For model #1, two coils are connected to the primary circuit in series, so the parameters for the secondary side (C_2, N_2, I_2, $|I_2/I_1|$ and, θ_{12}) remains blank. The power loss for this study only includes the winding loss of the IH coils. The losses due to the switching and internal resistance of the capacitors are not considered. To achieve the required output power, much higher current should be excited to the coil for the optimal model #1 due to lower number of turns to achieve the uniform temperature distribution. The currents focused on the coil influence the winding loss more than the decreased winding resistance, leading to lower efficiency of 73.03%. Thus, increasing number of turns with lower currents is more advantageous than lower number of turns with high currents. In contrast, the optimal model #2 enables to achieve higher efficiency of 82.09% as well as lower objective function value of 0.019. In model #3, the efficiency of 88% is guaranteed but the objective function value becomes higher than that of model #2, indicating the heat-source distribution more deviates from that obtained from the model #2.

In Fig. 12, the difference between model #2 and model #3 can be visually explained. The target heat-source distribution can be obtained well, especially in the model #2. The target requires higher heat-source near the edge of the magnetic workpiece, which is not susceptible to the magnetic flux due to a demagnetizing effect of the edge part so higher currents is required to achieve the target distribution. Therefore, the result in model #3 presents a reduced heat-source near the edge and this can lead to the enhanced efficiency.

TABLE 3. Design results of three optimized models.

Parameters	Model #1	Model #2	Model #3
Primary capacitor, C_1	1738 nF	696 nF	832 nF
Secondary capacitor, C_2	-	1925 nF	1728 nF
Drive frequency	100 kHz	100 kHz	100 kHz
Input voltage	15 V_p	10.0 V_p	9.6 V_p
Primary coil turns, N_1	8	12	10
Secondary coil turns, N_2	-	10	10
Primary coil current, I_1	30.81 A_p	7.68 A_p	8.87 A_p
Secondary coil current, I_2	-	19.44 A_p	14.20 A_p
Current ratio, $\lvert I_2/I_1\rvert$	-	2.53	1.60
Phase difference, θ_{12}	-	-74.22°	-59.00°
Winding loss	5.93 W	3.94 W	2.64 W
Objective function value	0.029	0.019	0.14
Efficiency	73.03%	82.09%	88.00%

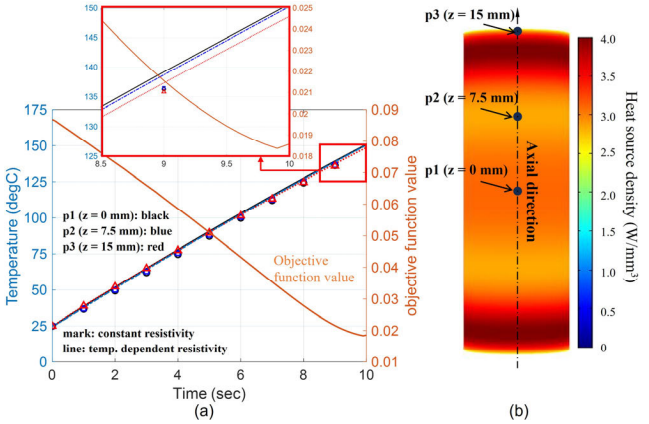

FIGURE 13. (a) Variations of the temperature and objective function value due to temperature-dependent resistivity of model #2 during a heating of 10 sec. (b) heat-source distribution along the workpiece at 150°C.

C. DISCUSSION

Though the proposed dual-coil design can be introduced in the previous part, there are still remaining challenges to improve the completeness and develop the more practical and competitive model. In a following section, the proposed design is compared with the dual-coil IH using dual inverters in terms of its strength and limitation from the economical and performance point of view. Additionally, two challenges due to temperature-dependent resistivity and magnetic nonlinearity, which are critical factors for prototyping the design model, are discussed to give a necessity of future works and an insight of research development to overcome challenges.

1) OPPORTUNITY AND CHALLENGE OF THE PROPOSED HEATING APPROACH

The proposed dual-coil design exhibits its superiority and limitation to the dual-coil IH fed by dual inverters and the conventional coil design fed by a single inverter as follows:

1) Relying only coil designs for achieving the desired heat-source distribution can result in lower efficiency, which is not appropriate for the applications where higher efficiency is imperative, specifically for numerous electronic devices energized by the battery.
2) The proposed system can mitigate the current stress on the inverter-side coil. Both model #2 and #3 show that the current amplitude of the primary coil, connected to the inverter, is lower than that of the secondary coil. The inverter can be connected to the secondary coil instead of the primary coil, enable selecting the coil where the lower current is required. This is advantageous to reduce the conduction loss of the inverter circuit.
3) From an economic point of view, the major component that determines the price of the driving circuit is due to the inverter consisting of a gate driver and MOSFETS. Specifically, the price of a half-bridge inverter IC (MP86905, Monolithic Power Systems) is $4.02 under massive order. In contrast, for the multilayer ceramic capacitor (MLCC), it costs about $0.05 which indicates that the proposed design results in halving the price of the driving circuit, compared to a dual-inverter system.
4) From the control point of view, the proposed dual-coil IH has a challenge to estimate the power consumption in the secondary coil, resulting in its difficulty for a flexible control during the heating process. In contrast, the dual-inverter system has its strength to estimate the input power injected into each coil more simply while an indirect prediction technique is required for proposed dual-coil IH, leading to more complex controls.

2) THE EFFECT OF TEMPERATURE DEPENDENT RESISTIVITY ON THE PROPOSED IH SYSTEM

First, the temperature-dependent resistivity still makes a challenge, especially in the field of control [19]. To analyze the influence of the temperature on the dual-coil IH system, coil arrays of model #2 and the workpiece with a supporter in Fig. 1 was used as a study model. The transient thermal analysis coupled with a time-harmonic magnetic simulation was conducted. In each simulation step, the resistivity was updated as a function of the temperature. Fig. 13(a) presents variations of the temperature and objective function value during the heating process. The temperature of three points along the workpiece, as illustrated in Fig. 13(b), is uniform from 0 $\sim$ 10 seconds even in the case that considered the temperature-dependent resistivity. The objective function values increase as the temperature deviates from 150°C where the optimization was conducted. The result indicates that variations of temperature distributions due to resistivity is not significant in this model (model #2) designed at one temperature point. Therefore, one specific target temperature can be selected for the optimal design, but the effect of the temperature-dependence on the current amplitude and phase should be considered and the discrepancy of the simulation and the prototype can be resolved through a tuning process.

Fig. 14 shows the effect of temperature on $|I_2/I_1|$, θ_{12}, and the output power. The temperature increases from 20°C

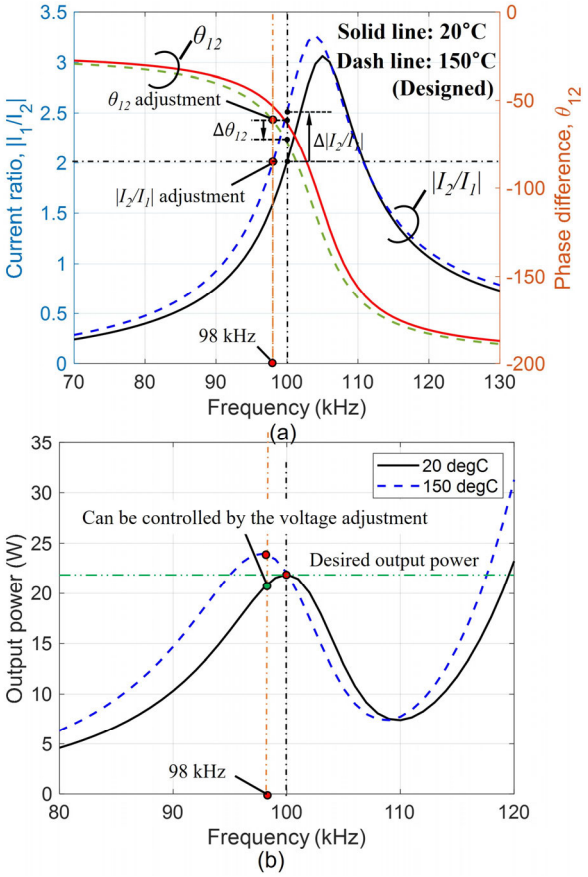

FIGURE 14. (a) Variations of $|I_2/I_1|$, θ_{12} and (b) output power according to the temperature of 20°C and 150°C (in the simulation).

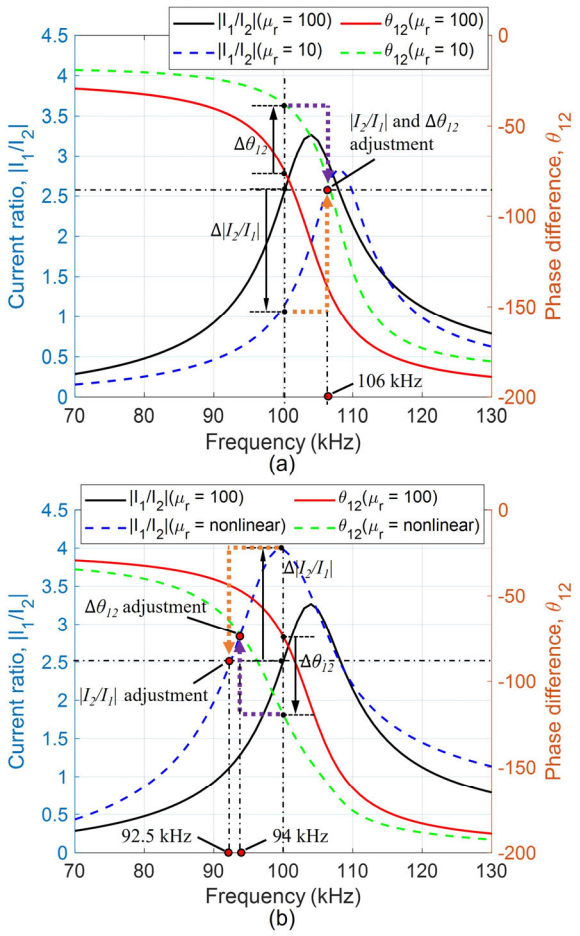

FIGURE 15. The variations on $|I_2/I_1|$ and θ_{12}, attributed to the different magnetic permeability, and the adjustment by changing the frequency: (a) relative permeability of 10 and 100 (in the simulation). (b) relative permeability of 100 and nonlinear permeability of the workpiece.

to 150°C change $|I_2/I_1|$ from 2.0 to 2.5, as well as θ_{12} from -73.78° to -62.90°, sensitive to the temperature in Fig. 14(a), resulting in making the temperature distribution deviated from target one. However, $|I_2/I_1|$ and θ_{12} can be compensated by adjusting the driving frequency, maintaining them to desired values and achieving the target temperature distribution. This result also addresses that $|I_2/I_1|$ and θ_{12} can be obtained despite of the uncertainty of the resistivity of the workpiece (material nature or temperature-dependence), which can make a discrepancy of the designed model with the prototyped model.

Additionally, the temperature distribution during the heating process can be controlled by adjusting the frequency, but the estimation technique of the power consumed in the secondary coil should be developed and implemented for controlling the power distribution between the primary and secondary coils. In Fig. 14(b), the output power also can be highly affected by the temperature, but the output power can be simply compensated by the voltage control.

3) THE EFFECT OF MAGNETIC PERMEABILITY ON THE PROPOSED IH SYSTEM

The magnetic nonlinearity can result in a discrepancy of the optimized model. Both $|I_2/I_1|$ and θ_{12} are sensitive to both an equivalent inductance and resistance of coils so additional fine tuning after manufacturing a product is necessary. To investigate the uncertainty of the permeability, three different permeabilities (10, 100, and nonlinear in [20]) are employed, and their effects on the resonance characteristics of $|I_2/I_1|$ and θ_{12} are calculated. In Fig. 15, both $|I_2/I_1|$ and θ_{12} are sensitive to permeability, so they deviate from the result of the initial design (relative permeability of 100). This can make large disagreement with the prototype at the fixed driving frequency of 100 kHz. When the frequency is adjusted from 100 kHz to 106 kHz, as shown in Fig. 15(a), the same combination of $|I_2/I_1|$ and θ_{12} can be achieved, compared to that obtained from the simulation ($\mu_r = 100$).

Fig. 15(b) shows the difference of frequency-dependent $|I_2/I_1|$ and θ_{12} when the relative permeability is 100 and non-linear. The result shows more deviations compared to that of Fig. 15(a). The frequency can be adjusted to make the same $|I_2/I_1|$ from 100 kHz to 92.5 kHz, and θ_{12} from 100 kHz to 94 kHz, indicating the small difference of the frequency. $|I_2/I_1|$ and θ_{12} at 92.5 kHz are 2.55 and -66°,

respectively, and θ_{12} deviates from the initially optimized result ($\theta_{12} = -74.22°$). Additionally, $|I_2/I_1|$ and θ_{12} at 94 kHz are 2.90 and -73.3°, respectively, and $|I_2/I_1|$ slightly deviates from the optimized result ($|I_2/I_1| = 2.53$). Thus, for robust design of the dual-coil IH system, the design process should consider the quality factor of the resonance circuit and the driving frequency to make both $|I_2/I_1|$ and θ_{12} less sensitive to frequency variations for the uncertainty-tolerance. Besides, for fine-tuning of the prototype, it is more advantageous to use a current amplitude than the phase angle so the driving frequency can be tuned to make $|I_2/I_1|$ the same as the designed value and subsequently, the voltage can be controlled to achieve the output power.

4) INITIAL PROTOTYPES AND FUTURE WORKS

Based on the previous discussion, an initial prototype coils are manufactured. Within the available MLCCs in the market, the primary and secondary capacitance are slightly changed from to 680 nF and 2,040 nF from the simulated values of 696 nF and 1,936 nF, respectively. For tuning the prototype model, the amplitude of the primary and secondary currents is measured and adjusted by changing the frequency from 100 kHz, an original design target. As a result, the frequency is adjusted to 107 kHz where the primary current, secondary current, and efficiency are 7.54 A, 16.57 A, and 83.05% respectively. The current ratio $|I_2/I_1|$ and phase difference θ_{12} are obtained as 2.20 and -51.1°, which was slightly deviated from simulated values of 2.53 and -74.22°.

As a result of the initial experiment, a main challenge of the fine-tuning for the prototype is its continuously variable temperature during heating, which leads to inconsistent tune if the temperature is not accurately measured simultaneously. Moreover, to copy with variable temperature, $|I_2/I_1|$ and θ_{12} must controlled and methodologies should be studied. For the future work, the thermocouple will be installed in the surface of the workpiece, as well as its controls to keep the $|I_2/I_1|$ and θ_{12} during whole heating cycle will be covered in the author's future article.

V. CONCLUSION

In this paper, we have studied the dual-coil IH system in the aspect of improving the flexibility of the temperature distribution optimization. The effect of both the current ratio and phase difference on the heat-source distribution was analyzed, and the resonance characteristics was presented to select suitable variables for the optimal design procedure. Then, the optimization algorithm was proposed and applied to the example IH model. The design result has validated that the dual-coil IH system can enhance the optimization more flexible, and the proposed design approach can increase the availability of IH technology. For the development of more practical device, some research developments for the future work are provided by author as follows:

- The prototype of the IH system where both temperature sensors and control methodologies will be developed, the manufacturing issues as well as the experimental validation will be covered in the author's future article.
- A generalized tuning procedure for the reproductivity of the prototype should be studied.
- A robust design approach of the proposed IH system for enhancing the uncertainty-tolerance caused by the manufacturing effect (structural and material properties)
- The estimation technique of the power consumed in the secondary coil should be developed.
- The optimization technique which can compromise the multiple objectives of the temperature distribution and efficiency and can find the parameters for the extended system using multiple coils.

REFERENCES

[1] J.-K. Byun, K. Choi, H.-S. Roh, and S.-Y. Hahn, "Optimal design procedure for a practical induction heating cooker," *IEEE Trans. Magn.*, vol. 36, no. 4, pp. 1390–1393, Jul. 2000.

[2] A. Boadi, Y. Tsuchida, T. Todaka, and M. Enokizono, "Designing of suitable construction of high-frequency induction heating coil by using finite-element method," *IEEE Trans. Magn.*, vol. 41, no. 10, pp. 4048–4050, Oct. 2005.

[3] N.-S. Choi, D.-W. Kim, and D.-H. Kim, "Optimal design of local induction heating coils based on the sampling-based sensitivity," *J. Korean Magn. Soc.*, vol. 23, no. 3, pp. 110–116, Jun. 2013.

[4] M. Kranjc, A. Županič, T. Jarm, and D. Miklavč ič, "Optimization of induction heating using numerical modeling and genetic algorithm," in *Proc. 35th Annu. Conf. IEEE Ind. Electron.*, Nov. 2009, pp. 2104–2108.

[5] P. Alotto, A. Spagnolo, and B. Paya, "Particle swarm optimization of a multi-coil transverse flux induction heating system," *IEEE Trans. Magn.*, vol. 47, no. 5, pp. 1270–1273, May 2011.

[6] Y. Gu, J. Xu, and T. Fu, "Design and optimization of coil structure based on the uniformity of core temperature field," *J. Mech. Sci. Technol.*, vol. 36, no. 6, pp. 2903–2912, Jun. 2022.

[7] H. P. Ngoc, H. Fujita, K. Ozaki, and N. Uchida, "Phase angle control of high-frequency resonant currents in a multiple inverter system for zone-control induction heating," *IEEE Trans. Power Electron.*, vol. 26, no. 11, pp. 3357–3366, Nov. 2011.

[8] H. N. Pham, H. Fujita, K. Ozaki, and N. Uchida, "Dynamic analysis and control for resonant currents in a zone-control induction heating system," *IEEE Trans. Power Electron.*, vol. 28, no. 3, pp. 1297–1307, Mar. 2013.

[9] K. Vishwas, K. Suryanarayana, and R. Acharya, "Modeling and simulation of multi coil induction heating system for semiconductor wafer processing," in *Proc. IEEE Int. Conf. Recent Trends Electron., Inf. Commun. Technol. (RTEICT)*, May 2016, pp. 588–592.

[10] W. Han, K. T. Chau, Z. Zhang, and C. Jiang, "Single-source multiple-coil homogeneous induction heating," *IEEE Trans. Magn.*, vol. 53, no. 11, pp. 1–6, Nov. 2017.

[11] E. Plumed, I. Lope, and J. Acero, "Induction heating adaptation of a different-sized load with matching secondary inductor to achieve uniform heating and enhance vertical displacement," *IEEE Trans. Power Electron.*, vol. 36, no. 6, pp. 6929–6942, Jun. 2021.

[12] W. Han, K. T. Chau, C. Jiang, and W. Liu, "All-metal domestic induction heating using single-frequency double-layer coils," *IEEE Trans. Magn.*, vol. 54, no. 11, pp. 1–5, Nov. 2018.

[13] D. Yun, H. Park, J.-H. Koo, S. Ham, and S. Lee, "Investigation of heat treatment of gears using a simultaneous dual frequency induction heating method," *IEEE Trans. Magn.*, vol. 51, no. 11, pp. 1–4, Nov. 2015.

[14] F. Guo, N. Tang, and I. P. Brown, "Combined dimensional and topology optimization of synchronous machine rotors using a material density interpolation method," *IEEE Trans. Ind. Appl.*, vol. 59, no. 6, pp. 6591–6600, Nov. 2023.

[15] D. Y. Um and G. S. Park, "Resistance variations in high-frequency inductors considering induced fields among conductors," *IEEE Trans. Magn.*, vol. 57, no. 2, pp. 1–5, Feb. 2021.

[16] R. Hughes, Y. Fan, and S. Dixon, "Near electrical resonance signal enhancement (NERSE) in eddy-current crack detection," *NDT E Int.*, vol. 66, pp. 82–89, Sep. 2014.
[17] Z. Novák and J. Kyncl, "Real time optimization of temperature field in induction heating," *J. Electr. Eng.*, vol. 70, no. 5, pp. 386–392, Nov. 2019.
[18] J. C. Lagarias, J. A. Reeds, M. H. Wright, and P. E. Wright, "Convergence properties of the nelder-mead simplex method in low dimensions," *SIAM J. Optim.*, vol. 9, no. 1, pp. 112–147, Jan. 1998.
[19] B. M. Gianesini, N. E. Cortez, R. A. Antunes, and J. Vieira Filho, "Method for removing temperature effect in impedance-based structural health monitoring systems using polynomial regression," *Structural Health Monitor.*, vol. 20, no. 1, pp. 202–218, Jan. 2021.
[20] N. Takahashi, M. Morishita, D. Miyagi, and M. Nakano, "Comparison of magnetic properties of magnetic materials at high temperature," *IEEE Trans. Magn.*, vol. 47, no. 10, pp. 4352–4355, Oct. 2011.

DAE YONG UM (Member, IEEE) received the B.S., M.Sc., and Ph.D. degrees in electrical engineering from Pusan National University, Busan, South Korea, in 2017, 2019, and 2023, respectively. He is currently a Research Associate with the Electric Power Group, Newcastle University, U.K. His research interests include numerical modeling and analysis of electromagnetic fields for electric machines, non-destructive testing, and wireless power transfer.

MIN JAE KIM received the B.S. and M.Sc. degrees in electrical engineering from Pusan National University, Busan, in 2018 and 2022, respectively. He is currently with LG Electronics. His research interests include induction heating and wireless power transfer.

SEUNG AHN CHAE received the B.S. degree in electrical engineering from Pusan National University, Busan, South Korea, in 2023, where he is currently pursuing the M.Sc. degree in electrical engineering. His research interests include electric machine design and non-destructive testing.

GWAN SOO PARK (Senior Member, IEEE) received the B.S., M.Sc., and Ph.D. degrees in electrical engineering from Seoul National University, Seoul, South Korea, in 1985, 1987, and 1992, respectively. From 1997 to 1999, he was a Visiting Scholar with Carnegie Mellon University. Since 2003, he has been a Professor with the School of Electrical and Computer Engineering, Pusan National University. From 2008 to 2009, he was a Visiting Scientist with Massachusetts Institute of Technology. His research interests include numerical modeling and analysis of electromagnetic fields for electric machines, non-destructive testing, and military applications.